Mon. Not. R. Astron. Soc. **000**, 000–000 (2007) Printed 18 August 2021 (MN LATEX style file v2.2)

# Bianchi Model CMB Polarization and its Implications for CMB Anomalies

Andrew Pontzen,[1⋆] Anthony Challinor[1,2]†
[1] *Institute of Astronomy, Madingley Road, Cambridge CB3 0HA, UK*
[2] *DAMTP, Centre for Mathematical Sciences, Wilberforce Road, Cambridge CB3 0WA, UK*

arXiv:0706.2075v2 [astro-ph] 7 Aug 2007

Accepted 2007 July 6. Received 2007 June 12.

**ABSTRACT**

We derive the CMB radiative transfer equation in the form of a multipole hierarchy in the nearly-Friedmann-Robertson-Walker limit of homogeneous, but anisotropic, universes classified via their Bianchi type. Compared with previous calculations, this allows a more sophisticated treatment of recombination, produces predictions for the polarization of the radiation, and allows for reionization. Our derivation is independent of any assumptions about the dynamical behaviour of the field equations, except that it requires anisotropies to be small back to recombination; this is already demanded by observations.

We calculate the polarization signal in the Bianchi $\mathrm{VII}_h$ case, with the parameters recently advocated to mimic the several large-angle anomalous features observed in the CMB. We find that the peak polarization signal is $\sim 1.2\,\mu$K for the best-fit model to the temperature anisotropies, and is mostly confined to multipoles $l < 10$. Remarkably, the predicted large-angle $EE$ and $TE$ power spectra in the Bianchi model are consistent with WMAP observations that are usually interpreted as evidence of early reionization. However, the power in $B$-mode polarization is predicted to be similar to the $E$-mode power and parity-violating correlations are also predicted by the model; the WMAP non-detection of either of these signals casts further strong doubts on the veracity of attempts to explain the large-angle anomalies with global anisotropy. On the other hand, given that there exist further dynamical degrees of freedom in the $\mathrm{VII}_h$ universes that are yet to be compared with CMB observations, we cannot at this time definitively reject the anisotropy explanation.

**Key words:** cosmic microwave background, cosmology: theory

## 1 INTRODUCTION

There are a number of observed features in the large-angle temperature anisotropies of the cosmic microwave background (CMB) that are anomalous under the usual assumption of statistically-isotropic, Gaussian fluctuations (see Copi et al. 2007 for a recent summary). Recent analyses have suggested that a small global anisotropy in the form described by Bianchi models could be to blame (Jaffe et al. 2005). In classical general relativity, the dimension of initial state space leading to models with such homogeneous anisotropies is always greater than the limitation of these models to the exactly isotropic case; furthermore, nearly isotropic models do not necessarily tend to late-time isotropy (Collins & Hawking 1973b). Although later work has suggested an inflationary epoch can be responsible for removing anisotropies (Wald 1983), this analysis is not complete (Goliath & Ellis 1999). It is therefore worth investigating further the observational predictions of such models; whilst to the skeptic they seem unlikely, the importance of a positive detection would be great.

Using the CMB models developed in Collins & Hawking (1973a) and Barrow, Juszkiewicz & Sonoda (1985), based on a specific solution for a type-$\mathrm{VII}_h$ universe with only pressureless matter, Jaffe et al. (2005) showed that known anomalies such as the low quadrupole amplitude, alignment of low-$l$ modes, large-scale power asymmetry and the 'cold spot' in the CMB could be mimicked. The work was extended in Jaffe et al. (2006) to include the dynamical effect of dark energy, yielding a degeneracy in the $\Omega_\Lambda$ - $\Omega_\mathrm{M}$ plane (which effectively arises through the angular diameter distance relation, since much of the temperature anisotropy is generated at high redshift). The degenerate range of parameters able to explain the large-angle anomalies was shown to be inconsistent with the cosmological parameters required to

⋆ Email: apontzen@ast.cam.ac.uk
† Email: a.d.challinor@ast.cam.ac.uk

© 2007 RAS

explain constraints such as supernovae observations and the CMB spectrum on smaller scales (i.e. the structure of the acoustic peaks). A more complete statistical analysis was performed by Bridges et al. (2007), in which the inconsistency of inferred parameters was confirmed.

There are remaining dynamical freedoms in the $\mathrm{VII}_h$ model which were not explored in the above papers. As noted in Jaffe et al. (2006), these will need investigation before any firm conclusions about the compatibility of the model with observations can be made.

A second important issue, hitherto not considered, is whether the predicted CMB *polarization* pattern in the Bianchi model that best fits the large-angle temperature anisotropies is consistent with current observations. The reason for its neglect seems to be that there are currently no full predictions for polarization in Bianchi models (Jaffe et al. 2006). In this paper, we address this issue by providing a complete and computationally convenient framework for calculating polarization in these models, and make a first attempt at confronting the predictions with the three-year data from the *Wilkinson Microwave Anisotropy Probe* (*WMAP*; Page et al. 2007). Polarization of the CMB in anisotropic cosmologies was first discussed by Rees (1968), where a calculation for Bianchi I models was outlined. Further consideration has been given to the problem in Matzner & Tolman (1982), where Bianchi types V and IX were considered. There are also a number of papers considering the effect of homogeneous magnetic fields on polarization (e.g. Milaneschi & Fabbri 1985; Fabbri & Tamburrano 1987), although we emphasize that the resulting Faraday rotation of the polarization is quite distinct from the purely gravitational effect under consideration here.

This paper is organized as follows. We briefly review Bianchi models in Section 2, including a more intuitive derivation of their FRW limit than has previously been published. In Section 3 we derive the zero order evolution of the photon polarization direction along geodesics, and incorporate these results into a multipole treatment of the Boltzmann equation that describes the radiative transfer in Section 4. Using this, we specialize our model to calculate the temperature and polarization anisotropies expected in a $\mathrm{VII}_h$ model with favoured parameters (Jaffe et al. 2006) in Section 5, and discuss the difficulties of reconciling the results with existing observations. We defer a full statistical reanalysis of Bianchi signatures, including reionization, to future work, where we will also explore more fully the extra dynamical degrees of freedom in the models.

## 2 BIANCHI MODELS

In this section we give a brief review of the framework that we use for our calculation. Anisotropic, homogeneous cosmological models can be classified according to the commutation relations of their spatial symmetry groups. The most popular classification method is based on Bianchi's (1897) classification of three-parameter Lie groups. For the development of these classifications in the cosmological context see Taub (1951); Heckmann & Schucking (1962); Estabrook, Wahlquist & Behr (1968); Ellis & MacCallum (1969), and for reviews see Wainwright (1997) and Ellis & van Elst (1998).

We adopt a $-+++$ metric signature, and will use Greek spacetime indices ($0 \to 3$) for tensor components in a general basis, early Latin indices ($a$, $b$ etc. running from $0 \to 3$) to label the vectors of any group-invariant tetrad, and middle Latin indices ($i$, $j$ etc. running from $1 \to 3$) to label spatial tetrad vectors in expressions only involving the spatial vectors. For the latter, we also use upper-case early Latin ($A$, $B$ etc.) when the tetrad is time-invariant (see below). As usual, round brackets denote symmetrisation on the enclosed indices and square brackets denote anti-symmetrisation.

A spacetime is said to be homogeneous if it can be foliated into space sections each admitting at least three linearly-independent Killing vector fields (KVFs) $\{\boldsymbol{\xi}\}$ (so that $\mathcal{L}_{\boldsymbol{\xi}}\mathbf{g} = 0$, where $\mathcal{L}$ denotes the Lie derivative and $\mathbf{g}$ is the metric tensor) with at least one subgroup that acts simply transitively in the space sections. We denote the elements of the three-dimensional subgroup by $\boldsymbol{\xi}_i$ where $i = 1$, 2, 3. The commutator of two KVFs is also Killing and, since the $\boldsymbol{\xi}_i$ form a subgroup, we must have

$$[\boldsymbol{\xi}_i, \boldsymbol{\xi}_j] = C^k_{ij}\boldsymbol{\xi}_k. \tag{1}$$

The $C^k_{ij} = C^k_{[ij]}$ are the structure constants of the Lie algebra of the group and are constant in space. (Through the foliation construction below they may also be shown to be constant throughout time.) The Jacobi identity,

$$[\boldsymbol{\xi}_i, [\boldsymbol{\xi}_j, \boldsymbol{\xi}_k]] + [\boldsymbol{\xi}_j, [\boldsymbol{\xi}_k, \boldsymbol{\xi}_i]] + [\boldsymbol{\xi}_k, [\boldsymbol{\xi}_i, \boldsymbol{\xi}_j]] = 0, \tag{2}$$

restricts the structure constants to satisfy

$$C^m_{n[i}C^n_{jk]} = 0. \tag{3}$$

Since a constant linear combination of KVFs will also be a KVF, one is permitted to perform global linear transformations:

$$\boldsymbol{\xi}_i \to \boldsymbol{\xi}'_i = T^j_i\boldsymbol{\xi}_j, \tag{4}$$

under which the structure constants transform as a (mixed) 3-tensor. Classifying all homogeneous spacetimes amounts to finding solutions to equation (3) that are inequivalent under the linear transformations (4).

The fiducial classification is achieved by decomposing the structure constants into irreducible vector and pseudotensor parts:

$$\begin{aligned} C^m_{ij} &= \epsilon_{ijk}n^{km} + a_i\delta^m_j - a_j\delta^m_i, \\ n^{ij}a_i &= 0 \qquad \text{(Jacobi identities)}, \end{aligned} \tag{5}$$

where $n^{ij}$ is symmetric and $\epsilon_{ijk}$ is the alternating tensor. Linear transformations can be used to diagonalise $n^{ij}$ and, since $a_i$ is an eigenvector of $n^{ij}$ one may take, without loss of generality:

$$\begin{aligned} n^{ij} &= \mathrm{diag}(n_1, n_2, n_3), \\ a_i &= (a, 0, 0). \end{aligned} \tag{6}$$

By rescaling (possibly reversing their directions) and relabelling the KVFs, we may reduce the structure constants to one of 10 distinct canonical forms that describe the 10 possible group types (see, for example, Ellis & MacCallum 1969). In these forms, all non-zero $n_i$ and $a$ are either $\pm 1$ except for the two types with $an_2n_3 \neq 0$ in which case there is an additional parameter $h \equiv a^2/(n_2n_3)$.

In order to express homogeneous tensor fields in an invariant way within this space, one must construct a suitable basis tetrad $\{\boldsymbol{e}_a\}$ that is invariant under the group action, i.e. satisfying

$$[\boldsymbol{e}_a, \boldsymbol{\xi}_i] = 0. \tag{7}$$

Any homogeneous tensor ($\mathsf{T}$ where $\mathcal{L}_{\boldsymbol{\xi}}\mathsf{T} = 0$) has components relative to this tetrad that are constant throughout space. The unit normal $\boldsymbol{n}$ to the hypersurfaces of homogeneity (satisfying $\boldsymbol{n} \cdot \boldsymbol{\xi}_i = 0$) is necessarily group-invariant ($[\boldsymbol{n}, \boldsymbol{\xi}_i] = 0$) via the Leibniz property of $\mathcal{L}$, so we can always take $\boldsymbol{e}_0 = \boldsymbol{n}$. Because of the foliated construction of the spacetime, one may label the hypersurfaces with a coordinate time $t$ such that $\boldsymbol{n}_\alpha = -t_{,\alpha}$ and hence $\boldsymbol{e}_0$ can be shown to be geodesic. In any homogeneous hypersurface, we can always construct the spatial part of the group-invariant tetrad by making an arbitrary choice for $\boldsymbol{e}_i$ at a point, and then dragging this frame out across the hypersurface with the $\boldsymbol{\xi}_i$ (see, for example, Ellis & MacCallum 1969).

In general the elements of the tetrad will not commute so one has

$$[\boldsymbol{e}_a, \boldsymbol{e}_b] = \gamma^c_{ab}\boldsymbol{e}_c, \tag{8}$$

where the $\gamma^c_{ab} = \gamma^c_{[ab]}$ are constant in the hypersurfaces of homogeneity by the Jacobi identities. The rotation coefficients encode the covariant derivatives of the tetrad:

$$\Gamma_{cab} \equiv e^\alpha_c e^\beta_a \nabla_\beta e_{b\alpha}, \tag{9}$$

where $e^\alpha_a$ are the components of the tetrad vectors in an arbitrary basis. The rotation coefficients are related to the $\gamma^c_{ab}$ by

$$\Gamma_{abc} = \frac{1}{2}\left(-\partial_a g_{bc} + \partial_b g_{ca} + \partial_c g_{ab} + \gamma_{abc} + \gamma_{cab} - \gamma_{bca}\right), \tag{10}$$

where $g_{ab} \equiv \mathsf{g}(\boldsymbol{e}_a, \boldsymbol{e}_b)$ are the tetrad components of the metric, $\gamma_{abc} \equiv g_{ad}\gamma^d_{bc}$ and $\partial_a$ is the ordinary derivative along the direction of $\boldsymbol{e}_a$. By taking $\boldsymbol{e}_0 = \boldsymbol{n}$, we have $g_{00} = -1$, $g_{0i} = 0$ and, since $\boldsymbol{n}$ is normalized, geodesic and irrotational, $\gamma^0_{ab} = 0$. The group-invariance of the tetrad restricts the form of the spatial components $\gamma^k_{ij}$: they are related to the group structure constants by a linear transformation and can be classified in the same way (and, necessarily, fall into the same Bianchi type: see MacCallum 1973).

It is always possible to construct the tetrad so that it is orthonormal; see Ellis & MacCallum (1969) for details. However, a convenient alternative is the *time-invariant frame* used by Collins & Hawking (1973a). In this case, the tetrad is constructed so that $[\boldsymbol{n}, \boldsymbol{e}_a] = 0$. The Jacobi identities applied to $\boldsymbol{n}$, $\boldsymbol{e}_a$ and $\boldsymbol{\xi}_i$ show that this is still consistent with the tetrad being group invariant. A specific construction is to start with a group-invariant tetrad over a hypersurface and to drag the tetrad along the normal $\boldsymbol{n}$ to cover spacetime. An important consequence is that the $\gamma^c_{ab}$ are constant throughout spacetime for the group-invariant tetrad. Moreover, $\gamma^i_{0j} = 0$ and the only non-vanishing components are spatial, i.e. $\gamma^k_{ij}$. Because the Bianchi classification of the Killing group and tetrad commutators is the same, it is always possible to perform a global (three-dimensional) linear transformation of the time-invariant tetrad to bring the $\gamma^k_{ij}$ equal to the canonical structure constants, i.e. $\gamma^k_{ij} = C^k_{ij}$. We shall use upper-case early Latin indices ($A$, $B$ etc.) to denote the spatial elements of this specific time-invariant tetrad.

The spacetime metric can then be written in terms of the time-invariant tetrad as

$$\mathsf{g} = -\boldsymbol{n} \otimes \boldsymbol{n} + g_{AB}(t)\boldsymbol{e}^A \otimes \boldsymbol{e}^B, \tag{11}$$

where the basis one-forms $e^A_\alpha = g^{AB}g_{\alpha\beta}e^\beta_B$ satisfy $e^A_\alpha e^\alpha_B = \delta^A_B$. Here, as usual, $g^{AB}$ denotes the inverse of $g_{AB}$. The $\boldsymbol{e}^A$ are also group- and time-invariant. We decompose the spatial part of the metric following Misner (1968):

$$g_{AB} = e^{2\alpha(t)}\left(e^{2\beta(t)}\right)_{AB}, \tag{12}$$

where $\beta$ is a matrix with zero trace and the matrix exponential is defined as usual via Taylor expansion, yielding $\det e^\beta = 1$. Thus $\alpha$ represents shape-preserving expansion whilst $\beta$ represents volume-preserving shape deformation. The expansion rate of the $\boldsymbol{n}$ congruence is $\nabla_\alpha n^\alpha = 3\dot{\alpha}$ and its shear – i.e. the trace-free, symmetric spatial projection of $\nabla_\alpha n_\beta$ – has components

$$\sigma_{AB} = \frac{1}{2}e^{2\alpha}\left(e^{2\beta}\right)^{\cdot}_{AB}. \tag{13}$$

Here, and throughout, overdots denote derivatives with respect to $t$. We shall make use of conformal time, $\eta$, defined by $\mathrm{d}t = e^\alpha \mathrm{d}\eta$, and we denote derivatives with respect to $\eta$ with primes.

The field equations are generally more naturally expressed in a (group-invariant) orthonormal frame, since the metric derivatives then vanish and one obtains first order equations for their commutation functions. The spatial vectors of such a frame will be represented with lower-case middle Latin indices, $i$, $j$ etc. One can always define a specific orthonormal frame by (Hawking 1969)

$$\boldsymbol{e}_i = e^{-\alpha}\left(e^{-\beta}\right)_{iA}\boldsymbol{e}_A. \tag{14}$$

The orthonormal tetrad is completed with $\boldsymbol{n}$. The components of the shear in the orthonormal frame are

$$\sigma_{ij} = (e^\beta)^{\cdot}{}_{k(i}(e^{-\beta})_{j)k}. \tag{15}$$

Note that this corresponds to the matter shear tensor only in the case that the fluid flow is not tilted relative to the hypersurfaces; i.e. the case $\boldsymbol{n} = \boldsymbol{v}$ where $\boldsymbol{v}$ is the fluid 4-velocity. In this paper, we do not specialize in this way.

### 2.1 FRW limit

It is instructive to sketch the derivation of the FRW limit of spacetimes in the time-invariant frame (the calculation in the orthonormal frame is described in Ellis & MacCallum 1969 and yields identical conditions).

A homogeneous spacetime can only be FRW if the expansion and 3-curvature are isotropic. Vanishing shear requires $\beta_{AB} = $ const. and then we can always set $\beta_{AB} = 0$ (i.e. diagonalise the spatial metric) with a constant linear transformation of the $\boldsymbol{e}_A$. After the transformation, the $\gamma^k_{ij}$ will no longer be equal to the canonical group structure constants (so we denote them with lower-case indices) but we can perform a further (constant) orthogonal transformation of the $\boldsymbol{e}_i$ (hence preserving $\beta = 0$) to bring the $\gamma^k_{ij}$ to the canonical form up to positive scalings of $a$, $n_1$, $n_2$ and $n_3$.

| Type | $a$ | $n_1$ | $n_2$ | $n_3$ | ${}^{(3)}Re^{2\alpha}$ |
|---|---|---|---|---|---|
| I | 0 | 0 | 0 | 0 | 0 |
| V | $-1$ | 0 | 0 | 0 | $-6$ |
| $\mathrm{VII}_0$ | 0 | 0 | 1 | 1 | 0 |
| $\mathrm{VII}_h$ | $-\sqrt{h}$ | 0 | 1 | 1 | $-6h$ |
| IX | 0 | 1 | 1 | 1 | 3/2 |

**Table 1.** Bianchi groups with FRW limit and their structure constants in canonical form. In the case $\mathrm{VII}_h$, we take $a=-\sqrt{hn_2n_3}$ for compatibility with the notation of Collins & Hawking (1973a) and Barrow et al. (1985). Note that $a$ can also be positive, but this case will be related by a rotation of the sky (constructed by $\boldsymbol{e}_1\to-\boldsymbol{e}_1$ followed by $\boldsymbol{e}_3\to-\boldsymbol{e}_3$) and need not be considered separately. However, the overall parity must be considered; one way is to consider the transformation $\boldsymbol{e}_1\to-\boldsymbol{e}_1$ which reverses the sign of $a$ and all $n_i$. The final column is the comoving 3-curvature scalar in the $\beta=0$ FRW limit.

With $\beta=0$, the 3-curvature is

$$\begin{aligned}{}^{(3)}R_{ij} &= \frac{1}{3}{}^{(3)}R\delta_{ij}e^{2\alpha}\\ &= -\frac{1}{4}\left[2\gamma^k_{il}\gamma^l_{jk}+2\gamma^l_{ki}\gamma^l_{kj}\right.\\ &\quad\left.-\gamma^i_{kl}\gamma^j_{kl}+2\gamma^k_{kl}(\gamma^i_{jl}+\gamma^j_{il})\right].\end{aligned}\tag{16}$$

Zero- and first-order expressions (such as the one above) will often contain surprising index placement; note that metric factors are always included where necessary to account for this.

In terms of the decomposition of $\gamma^k_{ij}$, one obtains the off-diagonal element ${}^{(3)}R_{23}=a(n_2-n_3)$, yielding the condition

$$a=0 \text{ or } n_2=n_3\tag{17}$$

if the curvature is to be isotropic. The vanishing of the remainder of the trace-free part further requires

$$n_1^2+n_2n_3=n_2^2+n_1n_3=n_3^2+n_1n_2,\tag{18}$$

which implies that at least one of the $n_i$ are zero and the remaining two are equal. By examining a complete list of distinct group types, these conditions yield the spaces with an FRW limit (Table 1). In each case we can use a volume rescaling (change of $\alpha$) to set the non-zero $n_i$ to unity or, if the $n_i$ vanish, $a$ to $-1$. This is enough freedom to set the $\gamma^k_{ij}$ of the time-invariant frame, with $\beta=0$, equal to the corresponding canonical group structure constants. For a universe that is close to FRW, we can therefore treat $\beta$ as a small perturbation while working in the time-invariant frame with $\gamma^C_{AB}$ still in canonical form.

## 3 PHOTON PROPAGATION

We parameterize the photon propagation direction vector according to the convention in Barrow et al. (1985); although this unusually places the azimuthal direction along $\boldsymbol{e}_1$, it more conveniently reflects the symmetries of the fiducial Bianchi classification, which ultimately yields much simpler equations. Thus in the *orthonormal* frame, the photon direction has components

$$p^i=(\cos\theta,\sin\theta\cos\phi,\sin\theta\sin\phi)\tag{19}$$

and the photon 4-momentum is

$$\boldsymbol{K}=E(\boldsymbol{n}+p^i\boldsymbol{e}_i),\tag{20}$$

where $E$ is the photon energy measured by an observer on a hypersurface-orthogonal path. It is convenient to introduce the comoving energy, $\epsilon\equiv Ee^{\alpha}$. In terms of this, the spatial components of $K$ on the time-invariant tetrad (in which the geodesic equations take their simplest form) are

$$K_A=\epsilon\left(e^{\beta}\right)_{iA}p^i.\tag{21}$$

The energy change along a geodesic follows from differentiating $E=-\boldsymbol{K}\cdot\boldsymbol{n}$. The geodesic equation then gives the exact result

$$\epsilon'=-\epsilon e^{\alpha}p^ip^j\sigma_{ij},\tag{22}$$

where $\epsilon'\equiv\mathrm{d}\epsilon/\mathrm{d}\eta$. This is equivalent to the integral result obtained by Hawking (1969). For the evolution of $\theta$ and $\phi$, we make use of the (exact) geodesic equation in the time-invariant frame (Barrow et al. 1985):

$$K_A'=\left(e^{-2\beta}\right)_{BD}\frac{K_CK_D}{\epsilon}C^C_{BA}.\tag{23}$$

We only require the evolution of $\theta$ and $\phi$ to zero order in $\beta$ since the radiation is necessarily isotropic in the FRW limit. Setting $\beta=0$ in equation (23), we find

$$\theta' = [a+(n_3-n_2)\cos\phi\sin\phi]\sin\theta\tag{24}$$

$$\phi' = [n_1-n_3+(n_3-n_2)\cos^2\phi]\cos\theta.\tag{25}$$

We denote the (complex) polarization 4-vector by $\boldsymbol{P}$. It is normalized so that $\boldsymbol{P}\cdot\boldsymbol{P}^*=1$ and, in the Lorentz gauge, is orthogonal to $\boldsymbol{K}$. The polarization $\boldsymbol{P}$ is parallel transported along the photon geodesic. We are more interested in the observed polarization $\tilde{\boldsymbol{P}}$ (i.e. the electric field direction for radiation in a pure state) relative to $\boldsymbol{n}$. This is given by screen-projecting $\boldsymbol{P}$ perpendicular to $\boldsymbol{n}$ and the photon direction $\boldsymbol{p}$:

$$\tilde{P}^{\alpha}=\mathcal{H}^{\alpha}{}_{\beta}P^{\beta},\tag{26}$$

where the screen-projection tensor $\mathcal{H}_{\alpha\beta}$ is defined by

$$\mathcal{H}_{\alpha\beta}\equiv g_{\alpha\beta}+n_{\alpha}n_{\beta}-p_{\alpha}p_{\beta}.\tag{27}$$

The evolution of $\tilde{\boldsymbol{P}}$ follows from the parallel transport of $\boldsymbol{P}$ itself (Challinor 2000):

$$\mathcal{H}^{\alpha}{}_{\beta}\left(K^{\rho}\nabla_{\rho}\tilde{P}^{\beta}\right)=0.\tag{28}$$

We find for the tetrad components of $\tilde{\boldsymbol{P}}$ in the time-invariant basis the exact equation

$$\dot{\tilde{P}}_A-\tilde{P}^B\sigma_{AB}-p_A\tilde{P}^Bp^C\sigma_{BC}-\dot{\alpha}\tilde{P}_A+p^B\tilde{P}^C\Gamma_{ABC}=0,\tag{29}$$

where $\Gamma_{ABC}$ are the rotation coefficients given by the spatial components of equation (10).[1] There is only one degree of freedom in the projected polarization vector, described by the angle between it and the $\hat{\boldsymbol{e}}_{\theta}$ direction:

$$\tilde{\boldsymbol{P}}=\hat{\boldsymbol{e}}_{\theta}\cos\psi+\hat{\boldsymbol{e}}_{\phi}\sin\psi\tag{30}$$

where $\hat{\boldsymbol{e}}_{\theta}$ and $\hat{\boldsymbol{e}}_{\phi}$ are constructed from the orthonormal-frame vectors. The components on the orthonormal frame are therefore

[1] The metric derivatives vanish in this case since $g_{IJ}$ is constant in each hypersurface.

$$\tilde{P}^i = \begin{pmatrix} -\sin\theta\cos\psi \\ \cos\theta\cos\phi\cos\psi - \sin\phi\sin\psi \\ \cos\theta\sin\phi\cos\psi + \cos\phi\sin\psi \end{pmatrix}. \quad (31)$$

The polarization is first-order in $\beta$ so we only require the evolution of $\psi$ at zero order. In this FRW limit, equation (29) reduces to

$$2\psi' = -n_1 - (n_3 - n_2)\cos 2\phi. \quad (32)$$

Since we are considering models close to FRW, $n_3 = n_2$ (see Table 1) and our evolution equations simplify to

$$\begin{aligned} \theta' &= -\sqrt{h}\sin\theta \\ \phi' &= (n_1 - n_3)\cos\theta \\ 2\psi' &= -n_1, \end{aligned} \quad (33)$$

where, for type V universes, one takes $\sqrt{h} = 1$. We see that the polarization only rotates relative to $\hat{\boldsymbol{e}}_\theta$ and $\hat{\boldsymbol{e}}_\phi$ in type-IX universes. These general equations for $\theta$ and $\phi$ agree with the specific cases given in Appendix B of Barrow et al. (1985); the general $\psi$ equation agrees with the previous analysis of type-IX universes given in Matzner & Tolman (1982).

## 4 BOLTZMANN EQUATION

In this section, we derive the first-order Boltzmann equation describing polarized radiative transfer in any Bianchi model with an FRW limit.

CMB polarization is generated by Thomson scattering and is therefore expected to be only linearly polarized. We can describe the radiation distribution function in terms of Stokes parameters $f$, $q$ and $u$ where $f$ gives the expected number density of photons per proper phase-space volume irrespective of their polarization state. The parameters $q$ and $u$ describe linear polarization relative to a basis that we take to be $\hat{\boldsymbol{e}}_\theta$ and $\hat{\boldsymbol{e}}_\phi$ for propagation along $p^i$. Then $(f+q)/2$ is the expected phase-space number density of photons that would be found in the $\hat{\boldsymbol{e}}_\theta$ linear-polarization state, and $(f+u)/2$ is the same for the state rotated by 45 deg (towards $\hat{\boldsymbol{e}}_\phi$). In the absence of scattering, $f$ is conserved along the photon path in phase space and $q$ and $u$ are conserved if referred to bases that rotate like $\tilde{\boldsymbol{P}}$ in equation (28). We parameterize $f$, $q$ and $u$ by the photon-direction angles $\theta$ and $\phi$ and by comoving energy $\epsilon$. Since these parameters are defined relative to a group-invariant tetrad, $f$ is independent of position in the hypersurfaces of homogeneity. The same is true for the Stokes parameters since the basis on which they are defined is constructed in an invariant manner.

The Lagrangian derivative of $f$ in phase space is

$$\frac{\mathrm{D}f}{\mathrm{D}\eta} = \frac{\partial f}{\partial\eta} + \frac{\partial f}{\partial\theta}\theta' + \frac{\partial f}{\partial\phi}\phi' + \frac{\partial f}{\partial\epsilon}\epsilon', \quad (34)$$

and is only non-zero because of scattering. The quantities $\epsilon'$, $\theta'$ and $\phi'$ are given by equations (22) and (33). Anisotropies are formed through the last term in equation (34) and by Thomson scattering off electrons with a non-zero peculiar velocity; both effects are first order. The remaining terms 'advect' the resulting pattern on the sphere using the zero-order transport equations. The energy dependence of the anisotropies is therefore proportional to $\epsilon\partial\bar{f}/\partial\epsilon$ where $\bar{f}$ is the Planck distribution function in the FRW background. We define the dimensionless temperature anisotropies $\Theta(\theta,\phi;\eta)$ by

$$f(\boldsymbol{K};\eta) = \bar{f}(\epsilon)\left(1 - \frac{\mathrm{d}\ln\bar{f}}{\mathrm{d}\ln\epsilon}\Theta\right). \quad (35)$$

Polarization is generated by scattering the anisotropies and, since Thomson scattering is achromatic, the polarization has the same $\epsilon$ spectrum as the anisotropies. We can therefore introduce dimensionless 'thermodynamic-equivalent' Stokes parameters $Q(\theta,\phi;\eta)$ and $U(\theta,\phi;\eta)$ as

$$(q \pm iu)(\boldsymbol{K};\eta) = -\frac{\mathrm{d}\bar{f}}{\mathrm{d}\ln\epsilon}(Q \pm iU). \quad (36)$$

The quantities $Q \pm iU$ have spin-weight 2, i.e. under a change of basis

$$\hat{\boldsymbol{e}}_\theta + i\hat{\boldsymbol{e}}_\phi \rightarrow e^{i\chi}(\hat{\boldsymbol{e}}_\theta + i\hat{\boldsymbol{e}}_\phi) \quad \Rightarrow \quad Q \pm iU \rightarrow e^{\pm 2i\chi}(Q \pm iU). \quad (37)$$

Expressed in this way, the time dependence of the temperature anisotropies obeys:

$$\frac{\partial\Theta}{\partial\eta} = \frac{\mathrm{D}\Theta}{\mathrm{D}\eta} - \frac{\partial\Theta}{\partial\theta}\theta' - \frac{\partial\Theta}{\partial\theta}\phi' - e^\alpha p^i p^j \sigma_{ij}, \quad (38)$$

where the first term on the right describes the Thomson scattering kernel (Section 4.3), the next two describe advection of the patterns on the sphere, and the final term is gravitational redshifting in the anisotropic expansion due to the shear. The advection terms are more transparent when interpreted as being due to the spatial dependence (relative to a parallel-propagated rather than time-invariant basis) transforming to angular dependence through free streaming. For polarization, we have

$$\begin{aligned} \frac{\partial(Q \pm iU)}{\partial\eta} &= \frac{\mathrm{D}(Q \pm iU)}{\mathrm{D}\eta} - \frac{\partial(Q \pm iU)}{\partial\theta}\theta' - \frac{\partial(Q \pm iU)}{\partial\phi}\phi' \\ &\quad \pm 2i(Q \pm iU)\psi', \end{aligned} \quad (39)$$

where the last term arises from polarization rotation. Again, the first term on the right describes Thomson scattering (see Section 4.3).

We expand the temperature anisotropies in terms of spherical harmonics about the propagation direction:

$$\Theta(\boldsymbol{p}) = \sum_{lm} \Theta_l^m Y_l^m(\boldsymbol{p}) \ . \quad (40)$$

For polarization, we expand in spin-weighted spherical harmonics[2] as

$$(Q \pm iU)(\boldsymbol{p}) = \sum_{lm} (E_l^m \pm iB_l^m)\, {}_{\pm 2}Y_l^m(\boldsymbol{p}). \quad (41)$$

Note that the Bianchi models are not parity invariant; the mirror universe can be obtained using the standard transformations

$$\begin{aligned} \Theta_l^m &\rightarrow (-1)^l \Theta_l^m \\ E_l^m &\rightarrow (-1)^l E_l^m \\ B_l^m &\rightarrow (-1)^{(l+1)} B_l^m \ , \end{aligned} \quad (42)$$

or, equivalently, flipping the signs of $a$ and all $n_i$ (which inverts the direction of the $\boldsymbol{e}_1$ axis).

[2] For a brief review, see Appendices A-C of Lewis, Challinor & Turok (2002).

### 4.1 Gravitational redshifting

The effect of the shear on the observed temperature pattern reads

$$\left(\frac{\partial\Theta}{\partial\eta}\right)_{\rm shear} = -e^\alpha p^i p^j \sigma_{ij}, \tag{43}$$

which is a pure quadrupole. In terms of spherical harmonics,

$$\begin{aligned}
\left(\frac{\partial\Theta_2^2}{\partial\eta}\right)_{\rm shear} &= \sqrt{\frac{2\pi}{15}}\left(\sigma_{33}-\sigma_{22}+2i\sigma_{23}\right)e^\alpha \\
\left(\frac{\partial\Theta_2^1}{\partial\eta}\right)_{\rm shear} &= \sqrt{\frac{8\pi}{15}}\left(\sigma_{12}-i\sigma_{13}\right)e^\alpha \\
\left(\frac{\partial\Theta_2^0}{\partial\eta}\right)_{\rm shear} &= -\sqrt{\frac{4\pi}{5}}\sigma_{11}e^\alpha \\
\left(\frac{\partial\Theta_2^{-m}}{\partial\eta}\right)_{\rm shear} &= (-1)^m\left(\frac{\partial\Theta_2^m}{\partial\eta}\right)^*_{\rm shear},
\end{aligned} \tag{44}$$

where $\sigma_{ij}$ are the components of the shear in the orthonormal frame. We see that shear injects power at $l=2$, but subsequent advection generally transports this to higher $l$.

### 4.2 Advection equations

The advection part of the Boltzmann equation for the temperature is

$$\left(\frac{\partial\Theta(\theta,\phi)}{\partial\eta}\right)_{\rm advec} \equiv -\frac{\partial\Theta(\theta,\phi)}{\partial\theta}\theta' - \frac{\partial\Theta(\theta,\phi)}{\partial\phi}\phi', \tag{45}$$

with $\theta'$ and $\phi'$ given by equations (33). Making use of the results

$$\begin{aligned}
\sin\theta\frac{\partial {}_sY_l^m}{\partial\theta} &= \frac{l}{l+1}\sqrt{\frac{[(l+1)^2-m^2][(l+1)^2-s^2]}{(2l+1)(2l+3)}}\,{}_sY_{l+1}^m \\
&\quad + \frac{ms}{l(l+1)}\,{}_sY_l^m - \frac{l+1}{l}\sqrt{\frac{(l^2-m^2)(l^2-s^2)}{(2l-1)(2l+1)}}\,{}_sY_{l-1}^m \\
\cos\theta\,{}_sY_l^m &= \frac{1}{l+1}\sqrt{\frac{[(l+1)^2-m^2][(l+1)^2-s^2]}{(2l+1)(2l+3)}}\,{}_sY_{l+1}^m \\
&\quad - \frac{ms}{l(l+1)}\,{}_sY_l^m + \frac{1}{l}\sqrt{\frac{(l^2-m^2)(l^2-s^2)}{(2l-1)(2l+1)}}\,{}_sY_{l-1}^m
\end{aligned} \tag{46}$$

which follow from standard recursion relations for the related Wigner functions $D^l_{-ms}(\phi,\theta,0)$ (e.g. Varshalovich, Moskalev & Khersonskii 1998), we find for the advective contribution to the time derivative of the multipoles

$$\left(\frac{\partial\Theta_l^m}{\partial\eta}\right)_{\rm advec} = \sum_{l'=l-1}^{l+1} f^m_{ll'}\Theta^m_{l'}. \tag{47}$$

Here,

$$\begin{aligned}
f^m_{l,l-1} &= \sqrt{\frac{l^2-m^2}{(2l-1)(2l+1)}}\left[im\Delta n + (l-1)\sqrt{h}\right] \\
f^m_{l,l} &= 0 \\
f^m_{l,l+1} &= \sqrt{\frac{(l+1)^2-m^2}{(2l+1)(2l+3)}}\left[im\Delta n - (l+2)\sqrt{h}\right]
\end{aligned} \tag{48}$$

with $\Delta n \equiv n_3 - n_1$. Note that ${}_\pm f^{-m}_{ll'} = {}_\mp f^{m*}_{ll'}$, as required by the reality of $\Theta(\theta,\phi)$ in equation (47).

For polarization, we have

$$\begin{aligned}
\left(\frac{\partial(Q\pm iU)}{\partial\eta}\right)_{\rm advec} &\equiv -\frac{\partial(Q\pm iU)}{\partial\theta}\theta' - \frac{\partial(Q\pm iU)}{\partial\phi}\phi' \\
&\quad \pm 2i\psi'(Q\pm iU).
\end{aligned} \tag{49}$$

We write

$$\left(\frac{\partial(E_l^m \pm iB_l^m)}{\partial\eta}\right)_{\rm advec} = \sum_{l'=l-1}^{l+1} {}_\pm g^m_{ll'}(E^m_{l'} \pm iB^m_{l'}), \tag{50}$$

which may be expressed

$$\begin{aligned}
\left(\frac{\partial E_l^m}{\partial\eta}\right)_{\rm advec} &= \frac{1}{2}\sum_{l'=l-1}^{l+1}\left[\left({}_+g^m_{ll'} + {}_-g^m_{ll'}\right)E^m_{l'}\right. \\
&\quad \left. + i\left({}_+g^m_{ll'} - {}_-g^m_{ll'}\right)B^m_{l'}\right], \\
\left(\frac{\partial B_l^m}{\partial\eta}\right)_{\rm advec} &= \frac{1}{2}\sum_{l'=l-1}^{l+1}\left[\left({}_+g^m_{ll'} + {}_-g^m_{ll'}\right)B^m_{l'}\right. \\
&\quad \left. - i\left({}_+g^m_{ll'} - {}_-g^m_{ll'}\right)E^m_{l'}\right].
\end{aligned} \tag{51}$$

We see that there are two modes of propagation; one transfers power amongst $l$ and the other mixes $E$ and $B$-modes. The mixing terms are

$$\begin{aligned}
{}_+g^m_{l,l} - {}_-g^m_{l,l} &= -2in_1 + \frac{4\left(\sqrt{h} - im\Delta n\right)m}{l(l+1)}, \\
{}_+g^m_{l,l+1} - {}_-g^m_{l,l+1} &= {}_+g^m_{l,l-1} - {}_-g^m_{l,l-1} = 0.
\end{aligned} \tag{52}$$

Polarization is generated from Thomson scattering as a pure electric quadrupole (see Section 4.3) but $B$-modes can subsequently be produced through advection. This happens in all nearly-FRW Bianchi models except type I. The $n_1$ term in equations (52) arises from the polarization rotation $\psi'$; the remaining terms are from the evolution of the photon direction relative to the invariant frame. For the power transfer, we find

$$\begin{aligned}
{}_+g^m_{l,l} + {}_-g^m_{l,l} &= 0, \\
{}_+g^m_{l,l-1} + {}_-g^m_{l,l-1} &= 2\sqrt{\frac{(l^2-m^2)(l^2-4)}{l^2(2l-1)(2l+1)}}\times \\
&\qquad \left[(l-1)\sqrt{h} + im\Delta n\right], \\
{}_+g^m_{l,l+1} + {}_-g^m_{l,l+1} &= 2\sqrt{\frac{[(l+1)^2-m^2]\,[(l+1)^2-4]}{(l+1)^2(2l+1)(2l+3)}}\times \\
&\qquad \left[-(l+2)\sqrt{h} + im\Delta n\right],
\end{aligned} \tag{53}$$

which are not affected by polarization rotation. Note that

$${}_\pm g^{-m}_{ll'} = {}_\mp g^{m*}_{ll'}, \tag{54}$$

as required by the reality of $E(\theta,\phi)$ and $B(\theta,\phi)$ in equation (50).

### 4.3 Scattering equations

We use a standard Thomson scattering kernel in the form derived by Hu & White (1997) (see also Dautcourt & Rose 1978):

$$\begin{aligned}
\left(\frac{D(E_l^m \pm iB_l^m)}{D\eta}\right) &= \tau'\left(-(E_l^m \pm iB_l^m)\right. \\
&\quad \left. + \frac{3}{5}\delta_{l2}(E_2^m - \frac{1}{\sqrt{6}}\Theta_2^m)\right),
\end{aligned}$$

$$\left(\frac{D\Theta_l^m}{D\eta}\right) = \tau'\Big(-\Theta_l^m(1-\delta_{l0}) + \frac{1}{10}\delta_{l2}(\Theta_2^m - \sqrt{6}E_2^m) + \delta_{l1}\tilde{u}_m\Big), \quad (55)$$

where $\tau' = n_e\sigma_t e^{\alpha}$ gives the scattering rate in conformal time, and

$$\begin{aligned}\tilde{u}_{-1} &= \sqrt{\frac{2\pi}{3}}(u_2 + iu_3)\\ \tilde{u}_0 &= \sqrt{\frac{4\pi}{3}}u_1\\ \tilde{u}_1 &= \sqrt{\frac{2\pi}{3}}(-u_2 + iu_3)\end{aligned} \quad (56)$$

are the dipole moments of the electron peculiar velocity in the orthonormal frame. It follows from equation (55) that Thomson scattering of the temperature quadrupole generates polarization that is an $E$-mode quadrupole.

## 5 IMPLEMENTATION FOR VII$_H$ UNIVERSES

### 5.1 Field equations

The complete set of field equations are available from, for example, Wainwright (1997). Naturally, these reduce at zeroth-order to the standard Friedmann and acceleration equations, so that

$$\begin{aligned}e^{\alpha_0}\frac{\mathrm{d}\eta}{\mathrm{d}z} &= \frac{-1}{H(z)}\\ &= -H_0^{-1}\left(\Omega_{\Lambda,0} + \Omega_{K,0}(1+z)^2 + \Omega_{\mathrm{M},0}(1+z)^3\right)^{-1/2},\end{aligned} \quad (57)$$

where $\Omega_{\mathrm{M},0}$, $\Omega_{\Lambda,0}$ and $\Omega_{K,0}$ have their usual meanings, $(1+z)^{-1} = e^{\alpha-\alpha_0}$ and $H = \dot{\alpha}$. The Friedmann constraint equation relates the group parameter $h$ to the curvature (see Table 1): $h = H_0^2 e^{2\alpha_0}\Omega_{K,0}$.

The evolution of the shear is required at first order and is provided by the trace-free part of the spatial evolution equations,

$$\dot{\sigma}_{ij} = -3H\sigma_{ij} - {}^{(3)}S_{ij} \quad (58)$$

in the orthonormal frame. Here,

$${}^{(3)}S_{ij} \equiv {}^{(3)}R_{ij} - {}^{(3)}R\delta_{ij}/3 \quad (59)$$

is the trace-free part of the intrinsic 3-curvature of the homogeneous hypersurfaces. Also, we have assumed a perfect fluid (i.e. zero anisotropic stress) and the shear equation (58) holds only at first order. It is convenient that, in the VII$_h$ case, ${}^{(3)}S_{12}$ and ${}^{(3)}S_{13}$ are zero to this accuracy, and, furthermore, no coefficient of $\beta_{12}$ or $\beta_{13}$ enters into the expression for ${}^{(3)}S_{ij}$, so that one may study a simple model in which $\sigma_{ij} = 0$ except for $\sigma_{12}, \sigma_{13} \propto e^{-3\alpha}$. The linear constraint equations show that the matter in such a model contains vorticity, i.e. the separation of neighbouring particles rotates relative to inertial gyroscopes.

Whilst it is not prohibitively difficult to implement a numerical solution for the most general case, we defer such a treatment to a later paper. Instead, we take advantage of the simplified solutions to derive the polarization in the favoured models of Jaffe et al. (2006).

We shall adopt the standard assumption that the CMB signal from global anisotropy adds linearly to that from inhomogeneities. This is clearly correct insofar as the linear-order perturbations are concerned; however, given that generic anisotropy modes grow towards the initial singularity, there is no guarantee that standard inflationary mechanisms for generating inhomogeneities can be invoked. Ignoring this potential inconsistency is pragmatic, but investigation would certainly be necessary if the resulting models gain any significant observational support.

### 5.2 Tilt decay

To be consistent with our assumption of small departures from FRW symmetry, we assume that all peculiar velocities are small. If we write the total momentum density of all matter and radiation as $\boldsymbol{P}^{(\mathrm{tot})} = \sum_n(\rho_{(n)} + p_{(n)})\boldsymbol{u}_{(n)}$, the linear constraint equation relates the spatial components to the shear:

$$8\pi P_i^{(\mathrm{tot})} = e^{-\alpha}(\sigma_{jk}C^j_{ki} - \sigma_{ij}C^k_{kj}) \quad (60)$$

to first order in the orthonormal frame. Here, the $C^i_{jk}$ are the structure constants in canonical form. In the restricted solution $\sigma_{12}, \sigma_{13} \propto e^{-3\alpha}$, so, assuming the total momentum density is dominated by a barotropic fluid with equation of state $p = w\rho$ for constant $w$, we have $\rho \propto e^{-3(1+w)\alpha}$ and

$$\begin{aligned}|\boldsymbol{u}| = (u_i u^i)^{1/2} &\propto e^{(3w-1)\alpha}\\ &\propto \begin{cases}\text{constant} & w = 1/3\\ e^{-\alpha} & w = 0.\end{cases}\end{aligned} \quad (61)$$

This behaviour of $|\boldsymbol{u}|$ is consistent with momentum conservation. To see this, consider the Euler equation for a non-interacting ideal fluid in the time-invariant frame. The fluid pressure is constant on surfaces of homogeneity but gradients proportional to $\dot{p}u_A$ appear in the fluid rest frame. These accelerate the fluid so that

$$\dot{p}u_A + (\rho + p)\dot{u}_A = 0. \quad (62)$$

Solving gives $u_A \propto e^{3w\alpha}$ and, recalling the zero-order metric $g^{AB} = e^{-2\alpha}$, we recover equation (61).

The above introduces a complication in multi-fluid models, which appears to have been overlooked in recent work. For two components, say, the tilt velocities $\boldsymbol{u}_{(1)}, \boldsymbol{u}_{(2)}$ need not be the same (except in the case of strong coupling). Only the total momentum density, $(\rho_1 + p_1)\boldsymbol{u}_{(1)} + (\rho_2 + p_2)\boldsymbol{u}_{(2)}$ is constrained by the shear so there is additional freedom in the solution.[3] Although the dark matter density will be dominant around the time of recombination, $z \sim z_{\mathrm{LSS}}$, the tilt velocity of relevance for the CMB is manifestly that of the baryons. Given that the baryons are tightly coupled to the photons until the last scattering surface, they experience a significant pressure and their tilt decay will be halted; this will not be the case for the dark matter. Thus,

[3] We note that, with this effect in mind, the application of the term 'universal vorticity' to describe VII$_h$ cosmologies is an over-simplification, since the vorticity of the dark matter need bear no resemblance to that of the baryons.

one needs to consider with care how to estimate the electron velocity in the Thomson scattering terms (56).

For most of cosmic history before recombination, the baryon–photon plasma has an equation of state parameter close to $w = 1/3$. A simple approximation is thus obtained by assuming the baryon tilt velocity remains constant before recombination, after which it decays as the inverse scale factor. If dark matter decouples at $z_{\rm DM}$, the ratio of baryon to dark-matter peculiar velocities at last scattering will be

$$\left.\frac{|\boldsymbol{u}_{(\rm b)}|}{|\boldsymbol{u}_{(\rm c)}|}\right|_{\rm LSS} \approx \frac{1+z_{\rm DM}}{1+z_{\rm LSS}}. \tag{63}$$

We take dark-matter decoupling to be at redshift (see e.g. Loeb & Zaldarriaga 2005)

$$z_{\rm DM} \sim \frac{10\,{\rm MeV}}{T_{\rm CMB}k_B}\left(\frac{M_\sigma}{100\,{\rm GeV}}\right)\left(\frac{M}{100\,{\rm GeV}}\right)^{1/4} \simeq 10^{11}, \tag{64}$$

where $k_B$ is Boltzmann's constant, $M_\sigma$ is the coupling mass, $M$ is the particle mass, and the chosen values assume a super-symmetric origin of the CDM particle.

Unfortunately, the linearisation will break down at high redshift as the expansion-normalized scales as $e^{-\alpha}$, so the value by which the dark matter tilt is suppressed relative to the baryon tilt is unclear. However, equation (63) strongly suggests that the baryon–photon plasma dominates the momentum density at last scattering and that its tilt should be properly determined at $z_{\rm LSS}$ by equation (60) with $\boldsymbol{P} = (\rho_{\rm b} + 4\rho_\gamma/3)\boldsymbol{u}_{(\rm b)}$ on the left-hand side. After this $\boldsymbol{u}_{(\rm b)}$ decays as $1+z$ as determined by (62). The usual procedure of assuming that all components have the same tilt underestimates $|\boldsymbol{u}_{(\rm b)}|$ at last scattering by the ratio of the baryon–photon enthalpy to the total enthalpy. For the majority of our results, we follow the usual procedure for consistency with previous work. We consider the effect of the improved velocity analysis in Section 5.7, where we show that it will have a significant impact on statistical studies, but does not change our qualitative results.

### 5.3 Parameters of the model

For ΛCDM, the background model may be specified fully by the physical densities in CDM ($\omega_{\rm c,0} \equiv \Omega_{\rm c,0}h_{100}^2$ with $H_0 = 100h_{100}\,{\rm km\,s^{-1}\,Mpc^{-1}}$) and baryons ($\omega_{\rm b,0}$) with $\Omega_{\Lambda,0}$ and $\Omega_{K,0}$. The Hubble constant and $\Omega_{\rm M,0}$ are then derived quantities. Models with fixed $\omega_{\rm c,0}$ and $\omega_{\rm b,0}$ have the same early-universe history and reproduce the same acoustic peak structure in the CMB spectra if the angular-diameter distance to last-scattering and the primordial power spectra are additionally held fixed (Efstathiou & Bond 1999). The Bianchi representation with structure constants in canonical form further requires us to specify $e^{\alpha_0}$, although this is of no physical consequence in the background. In the perturbed model, the current scale factor $e^{\alpha_0}$ determines the physical size over which the shear eigenvectors rotate in space on a parallel-propagated triad. For the simplified perturbed model, we must additionally specify initial values for $\sigma_{12}$ and $\sigma_{13}$. Due to the rotational symmetry of the $\mathrm{VII}_h$ structure constants about $\boldsymbol{e}_1$, only $m = \pm 1$ anisotropies and polarization are generated in this model, and are proportional to $[(\sigma_{12} \mp i\sigma_{13})/H]_0$ respectively. Varying the phase of $\sigma_{12}+i\sigma_{13}$ amounts to rotating the sky about $\boldsymbol{e}_1$ (reflecting the residual freedom in the choice of $\boldsymbol{e}_2$ and $\boldsymbol{e}_3$), while the rotationally-invariant content depends on $\sigma_{12}^2 + \sigma_{13}^2$. We can, therefore, always choose $\sigma_{12} = \sigma_{13}$ which we do for compatibility with previous studies.

The morphology of the CMB anisotropy and polarization patterns in the Bianchi model is determined largely by the parameters $\Omega_{\rm M,0}$, $\Omega_{\Lambda,0}$ and the conformal Hubble parameter $e^{\alpha_0}H_0$. The expansion-normalized shear $(\sigma_{12}/H)_0$ and $(\sigma_{13}/H)_0$ determine the amplitude.[4] Collins & Hawking (1973a) denote the conformal Hubble parameter by $x$, i.e.

$$x = \dot{\alpha_0}e^{\alpha_0} = \sqrt{\frac{h}{\Omega_{K,0}}}, \tag{65}$$

where the latter relation arises directly from the FRW definition of $\Omega_{K,0}$, with $K = -h$ in our case (Section 2.1). With $x$, $\Omega_{\rm M,0}$ and $\Omega_{\Lambda,0}$ fixed, variations in $e^{\alpha_0}$ change physical scales in the model (e.g. the age) but do not affect the conformal properties. There is an approximate degeneracy amongst $\Omega_{\rm M,0}$, $\Omega_{\Lambda,0}$ and $x$ that preserves the morphology of the Bianchi patterns (Jaffe et al. 2006; Bridges et al. 2007). In our results, we follow Jaffe et al. (2006) by fixing $\omega_{\rm c,0}$ and $\omega_{\rm b,0}$ and use an ionization history consistent with these choices. Further specifying $\Omega_{\rm M,0}$ and $\Omega_{\Lambda,0}$ determines $H_0$; the current scale factor is then fixed by $x$.

### 5.4 Summary of the calculation

We assemble a hierarchy of multipole equations for $\Theta_{lm}$, $E_{lm}$ and $B_{lm}$ using the results of Section 4. The Thomson scattering rate $\dot{\tau}$ requires a model for the recombination (and potentially reionization) history, for which we use RECFAST (Seager, Sasselov & Scott 1999).

Starting at $z \simeq 1500$, the initial power is taken to be zero for the polarization, with a pure dipole for the temperature arising from the tilt of the baryon–photon fluid. Whilst the universe remains optically thick, a small quadrupole term in the temperature and polarization distributions arises from the equilibrium between scattering and anisotropic redshifting due to shear; this is quickly attained during the numerical integration and there is no requirement to include it in the initial conditions. However, we verified that starting significantly earlier ($z \simeq 1800$) made no difference to the final results.

Since the power in the temperature modes declines very rapidly for $l > 15$, we truncate the hierarchy at $l = 60$ without any special boundary conditions. Performing the calculation with a higher truncation ($l = 120$) made no difference to the results for $l < 30$. During the numerical integration we ensure at each timestep $\delta\eta \ll 1$, $\sigma\delta\eta \ll 1$ and $\dot{\tau}\delta\eta \ll 1$.

We investigate the polarization properties of the CMB in two models on the degeneracy proposed by Jaffe et al. (2006), namely $(x, \Omega_{\Lambda,0}, \Omega_{\rm M,0}) = (0.62, 0, 0.5)$ and $(1.0, 0.7, 0.2)$ respectively, both with "right-handed" parity. The latter model is as close to a concordance value as

[4] The more refined treatment of tilt velocities requires one to specify also the fraction of baryons to dark matter and the physical Hubble parameter. However, the Doppler terms are generally only a small correction to the anisotropy accumulated through the shear. The details of recombination introduce further dependencies on the physical densities of baryons and dark matter.

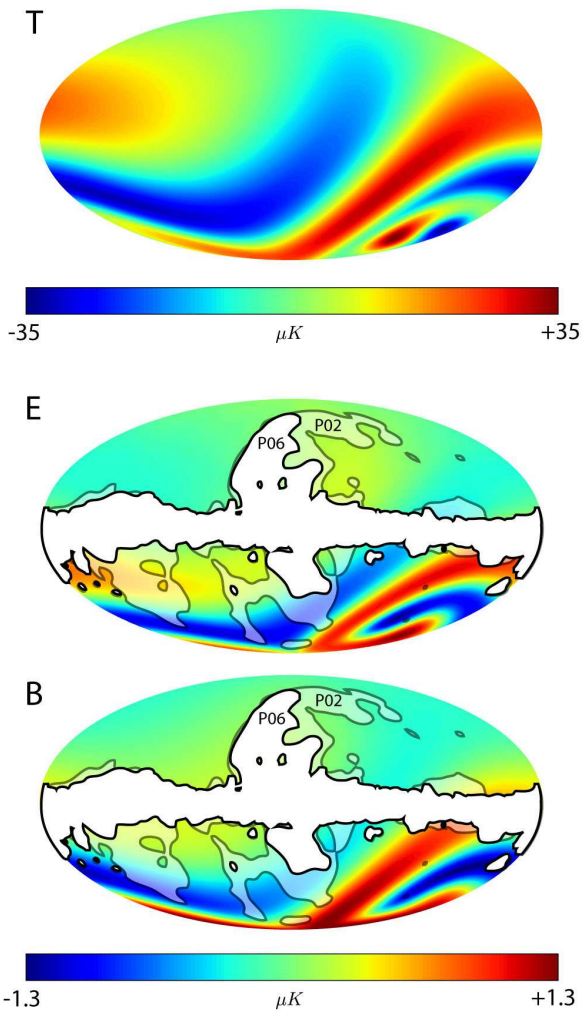


**Figure 1.** Temperature (top), $E$-mode (middle) and $B$-mode polarization (bottom) maps for the Bianchi VII$_h$ model with $(x, \Omega_{\Lambda,0}, \Omega_{\mathrm{M},0})$=$(0.62, 0, 0.5)$ and a consistent recombination history and no reionization. The maps have been transformed to the observational basis $(-\boldsymbol{p}, \hat{\boldsymbol{e}}_\theta, \hat{\boldsymbol{e}}_\phi)$, which involves a parity change of the form (42), and rotated to match the orientation of the template given in Jaffe et al. (2006). The masks used in the *WMAP* polarization analysis (Page et al. 2007) are overlaid on the polarization maps.

the Bianchi fitting allows (see Fig. 7 in Bridges et al. 2007). In both cases, we take $\omega_{\mathrm{b},0} = 0.022$ and $\omega_{\mathrm{c},0} = 0.110$ and the consistent recombination history with no reionization. These models produce almost identical polarization patterns, for reasons outlined below. We briefly discuss the effects of altering the ionization history in various ways (including reionization) in Section 5.6.

In each case, we normalize such that the maximum temperature anisotropy corresponds to $\Delta T = \pm 35\,\mu$K. Note that the amplitude of the polarization anisotropy simply scales linearly with the magnitude of the temperature anisotropy.

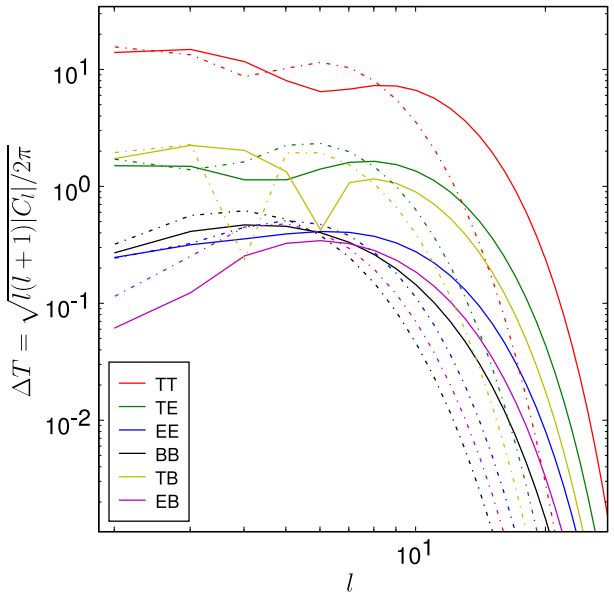


**Figure 2.** Auto- and cross-correlation power spectra for the Bianchi models $(x, \Omega_{\Lambda,0}, \Omega_{\mathrm{M},0}) = (0.62, 0, 0.5)$ (solid lines) and $(x, \Omega_{\Lambda,0}, \Omega_{\mathrm{M},0}) = (1.0, 0.7, 0.2)$ (dotted lines), normalized such that the maximum $\Delta T = \pm 35\,\mu$K. (The units of the vertical axis are $\mu$K.) The main difference between the models is a shift of power to larger scales (lower $l$) in the model with $\Lambda$; this is well understood in terms of the reduced focusing given lower $\Omega_{K,0}$ (see text), and causes no difference to our conclusions. Note that the $TB$ correlation is negative for $l < 6$ and $l < 5$ in the respective models.

### 5.5 Results

The resulting temperature and polarization $E$- and $B$-mode maps for the $\Omega_{\Lambda,0} = 0$ case are illustrated in Fig. 1. The level of the polarization is very high, approximately 1 $\mu$K. Heuristically, this is because the shear modes considered here decay as $(1+z)^3$, so that a substantial portion of the final temperature anisotropy can be built up between individual scattering events at high redshift. Because of the efficient conversion of $E$-modes to $B$, (equation 52), the $B$-mode contribution is of similar magnitude to the $E$-mode.

Although computing the power spectra,

$$C_l^{XY} = \frac{1}{2l+1} \sum_m a_{lm}^{X*} a_{lm}^{Y}, \tag{66}$$

does throw away useful information in these models, it provides a fast and efficient way to compare our results with known, and robust, polarization constraints. Since the multipole hierarchy does not transfer power between different $m$ values, and the implemented cosmology only generates anisotropies with $m = \pm 1$, in forming the power spectrum we are throwing away only phase information.

Given the position of the Bianchi-like features on the sky given in Jaffe et al. (2006), we may be confident that the P06, and even the P02, mask of the *WMAP* polarization analysis (Page et al. 2007) could not hide the polarization signal to a great extent (Fig. 1). Although the relation between the Stokes parameters and $E$ and $B$ is non-local, we note that maps of the Stokes parameters have their power localized in a similar way to $E$ and $B$ (and $T$). We therefore

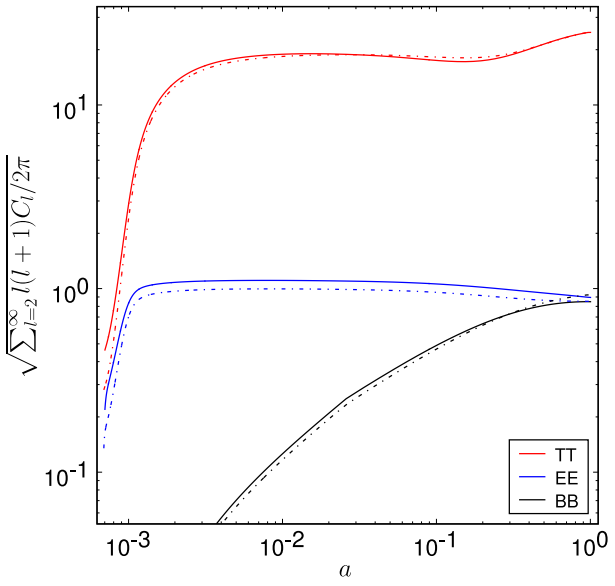


**Figure 3.** Growth of observable r.m.s. signal in the $T$ and $E$- and $B$-mode polarization plotted against $a = e^{\alpha-\alpha_0} = (1+z)^{-1}$ for the models $(x, \Omega_{\Lambda,0}, \Omega_{\mathrm{M},0})$=$(0.62, 0, 0.5)$ (solid lines) and $(x, \Omega_{\Lambda,0}, \Omega_{\mathrm{M},0})$=$(1.0, 0.7, 0.2)$ (dotted lines). Note that the power grows rapidly at high redshift while the shear is still significant, then remains constant (although it is transferred to higher $l$, which cannot be seen in this diagram). It is for this reason that the polarization is remarkably strong and relatively insensitive to the cosmology along the line for which the VII$_h$ temperature patterns are degenerate.

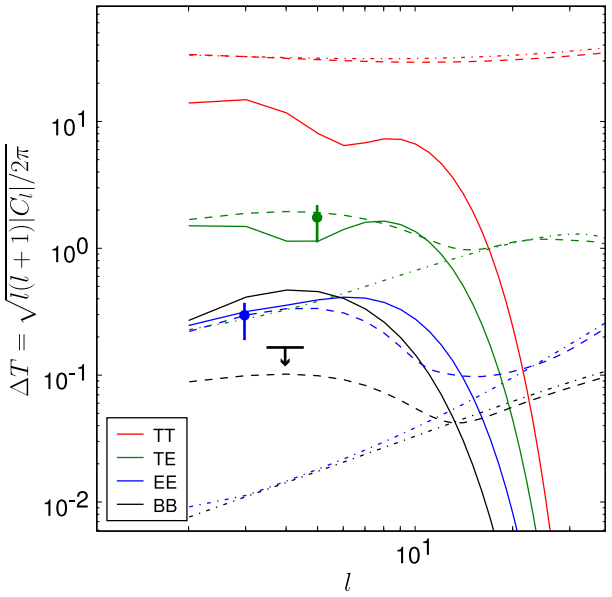


**Figure 4.** Bianchi VII$_h$ induced power in the CMB (solid lines) for $(x, \Omega_{\Lambda,0}, \Omega_{\mathrm{M},0})$=$(0.62, 0, 0.5)$ and no reionization, compared with Gaussian power from inhomogeneities for $(\omega_{\mathrm{c},0}, \omega_{\mathrm{b},0}, \sigma_8, r) = (0.110, 0.022, 0.7, 0.3)$ with reionization optical depth $\tau = 0$ (dash-dotted lines) and $\tau = 0.10$ (dashed lines). The polarization data are from the *WMAP* three-year release (Page et al. 2007). From the $TE$ and $EE$ power spectra alone, the Bianchi-induced polarization can mimic the effect of early reionization in the standard scenario (the conventional interpretation of the large-scale polarization power seen by *WMAP*). However, the best-fit Bianchi model to the temperature map clearly over-produces $B$-mode power compared to the *WMAP* upper limit (plotted) ruling out the simple model immediately.

calculate the full-sky power spectra without any consideration of the effect of masking nor the weighting with the inverse of the (non-diagonal) pixel-pixel noise covariance matrix that were employed by the *WMAP* team. Given that the r.m.s. Bianchi signal inside the masks is lower than outside, we expect the effects of masking would increase the estimated Bianchi power spectra over the full-sky values plotted in Fig. 2.

The major difference between the two parameter sets considered is that, for the $\Omega_{\Lambda,0} = 0.7$ case, the distinctive spiral pattern is less 'focused'. This is a well understood effect of reducing the spatial curvature $\Omega_{K,0}$ to 0.1 from its original value, 0.5 (e.g. Barrow et al. 1985), and manifests itself as a shift of power to lower $l$ (see Fig. 2). The existing statistical studies show that distinguishing these cases observationally is currently not possible (Bridges et al. 2007).

There is no significant difference in the overall polarization power. This follows because the majority of the power is built up rapidly at high redshifts as the universe becomes optically thin and the shear term has not decayed: at this point, the model is insensitive to the values of $\Omega_{\Lambda,0}$ and $\Omega_{K,0}$ (Fig. 3). Allowing $\omega_{\mathrm{b},0}$ to vary introduces much more substantial variations in the relative level of polarization; however, this introduces a further degree of freedom and is beyond the scope of our current analysis.

In Fig. 4, we compare the power spectra in the Bianchi $\Omega_{\Lambda,0} = 0$ model with the power expected in a 'concordance' model with standard, statistically-isotropic and homogeneous perturbations. The latter spectra are computed using CAMB (Lewis, Challinor & Lasenby 2000) for two models, one with no reionization (dot-dashed lines) and a favoured reionization model (dashed lines; $\tau = 0.10$). Forming combined power spectra by adding the power from the Bianchi model that best fits the temperature maps to that from the concordance model is inconsistent, since the models have different parameters (Bridges et al. 2007). However, ignoring this problem and comparing the models as 'templates' shows that, so far as the $TE$ and $EE$ power spectra are concerned, the Bianchi model can mimic the observed large-angle power that is conventionally attributed to reionization. Of course, the 'corrected' power in such a model would probably lead to an unfeasibly low estimate for $\tau$ in light of other data such as the Gunn-Peterson constraints (e.g. Fan, Carilli & Keating 2006). So, at least with the fiducial simplified dynamics outlined in Section 5.1, this already provides strong evidence against the VII$_h$ model.

More challenging for the Bianchi model is the $B$-mode polarization, which is at a similar level to the $E$-mode. In Page et al. (2007), the $B$-modes for $l < 10$ are found to be consistent with zero with errors better than $\sigma \sim 0.1\,\mu\mathrm{K}^2$ at each multipole. At this level, the signal-to-noise on the $B$-mode spectrum in the Bianchi model should be at least unity for *each* $2 < l < 8$, and would have produced a highly significant detection of large-angle $B$-modes overall.

Finally, the Bianchi models are not parity-invariant and one therefore obtains a $TB$ and $EB$ cross-correlation

(Fig. 2). To get a rough estimate of the current statistical power of these spectra in constraining the Bianchi model, we compute the $\chi^2$ between the model prediction and the *WMAP* estimates of $C_l^{TE}$ and $C_l^{TB}$ available on the LAMBDA website[5]. We use the spectra from $l = 2$–16 and, since only the diagonal errors are publically available, we ignore correlations between the estimates and complications due to the shape of the low-$l$ likelihood. As noted earlier, we also ignore the effects of foreground masking and noise-weighting.[6] We find reduced $\chi^2$ values of 0.5 for $TB$ and 4.3 for $EB$ for 15 degrees of freedom. The corresponding figures for null $C_l^{TB}$ and $C_l^{EB}$ are 0.4 and 0.6. Note that, although the Bianchi power is typically two orders of magnitude smaller in $EB$ than $TB$, the $EB$ estimates have smaller errors as $C_l^T$ exceeds the variance of the polarization noise on these scales. The interpretation of these $\chi^2$ values is that the data are too noisy to distinguish the Bianchi model from the null case for $TB$ (both are perfectly consistent) but the $EB$ spectra disfavour the Bianchi model over the null case.

### 5.6 Effect of ionization history

Since the shear decays rapidly, $\sigma \propto (1+z)^3$, our inclusion of a more detailed recombination calculation will affect the temperature maps somewhat. We take the $\Omega_{\Lambda,0} = 0$ model and run the Boltzmann hierarchy twice; first with instantaneous recombination at $z = 1100$ and then with the full RECFAST history (with no reionization). There is no qualitative difference in the temperature maps produced, but there is an approximately 15 percent decrease in the temperature amplitude in the latter case. Of course, this is simply reflected in a slightly different estimate of $(\sigma/H)_0$ and has no significant impact on previous probes of Bianchi signatures.

However, the detailed recombination history does have a significant impact on the amplitude of polarization. With the detailed model, the amplitude is approximately five times larger than that derived from the instantaneous model. Note that this puts the amplitude of polarization in the instantaneous model in agreement with the estimation in Rees (1968). It is unsurprising that the polarization is so sensitive to the recombination model, given that it arises through the detailed interplay of the rapidly decreasing shear and sharply peaked visibility function $\dot{\tau}e^{-\tau}$.

The effect of adding reionization is not as dramatic as for standard FRW perturbations; this is because of the high level of the primordial polarization relative to the temperature signal ($\sim 1/25$) on large scales. Adding reionization as early as $z = 15$ produces only a $\sim 50$ percent increase in the $EE$ power.

### 5.7 Effect of improved constraint model

The numerical results presented so far have derived the baryon tilt assuming the same tilt for all particle species,

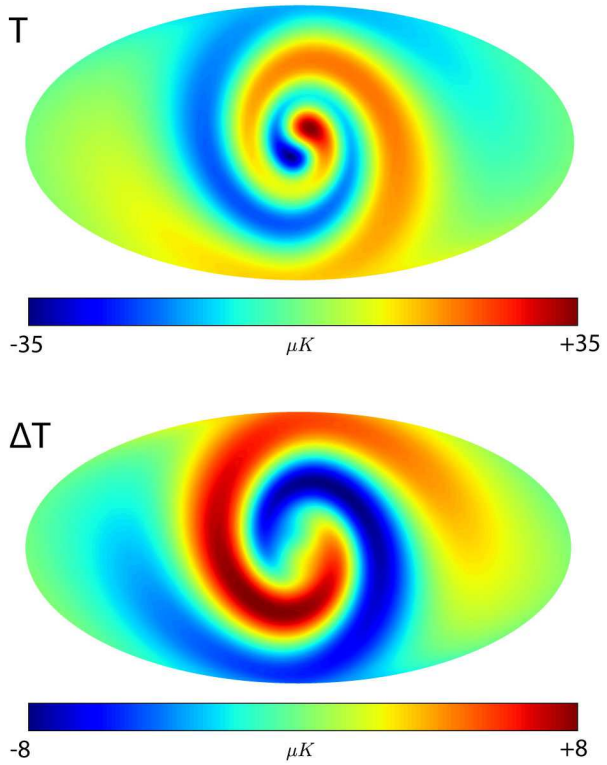


**Figure 5.** (Top) Normalized temperature map for Bianchi VII$_h$ model $(x, \Omega_{\Lambda,0}, \Omega_{\mathrm{M},0})$=(0.62, 0, 0.5) with improved tilt constraint; (bottom) residuals in this map compared to the standard constraint map (Fig. 1). The centre of the maps are here oriented down the $\boldsymbol{e}_1$ axis.

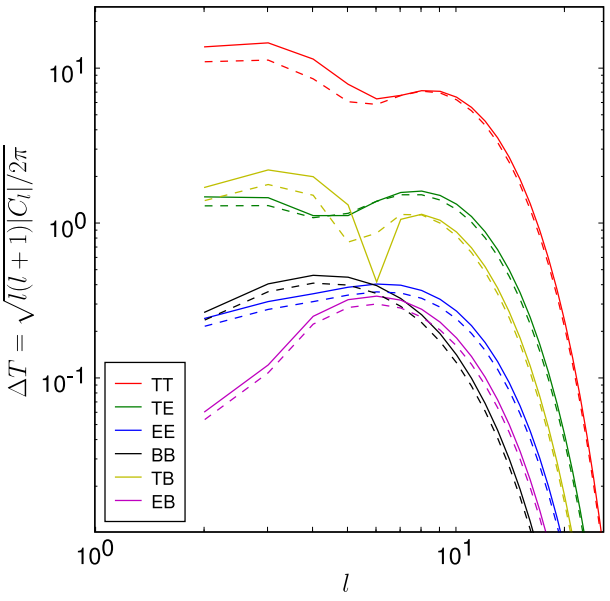


**Figure 6.** Comparison of power spectra with standard constraint (solid lines) and improved constraint (dashed lines) after renormalizing the maximum temperature anisotropy to $\pm 35\,\mu$K.

[5] `http://lambda.gsfc.nasa.gov/`

[6] We checked that the additional variance in the power spectrum estimates (when averaging over statistically-isotropic CMB fluctuations and noise) due to products between the two-point functions of the Bianchi signal and fluctuations is only a small correction to the errors computed by the *WMAP* team.

consistent with previous work. In this section, we analyze the effect of dropping this assumption and adopting the more sophisticated model of Section 5.2.

One may see heuristically that the shear generally contributes more to the temperature anisotropy than the dipole, because its integrated effect (for models with matter domination over most of the line of sight) scales as $\sim \Omega_{\mathrm{M},0}^{-1/2}(\sigma/H)_0(1+z_{\mathrm{LSS}})^{3/2} \times \mathcal{O}(1)$ whereas the dipole is imprinted instantaneously at scattering and scales in the improved model as

$$|\boldsymbol{u}| \sim \frac{\sqrt{1+9h}(1+z_{\mathrm{LSS}})}{x\Omega_{\mathrm{b},0}} \left(\frac{\sigma}{H}\right)_0 . \tag{67}$$

Using this new approach with the two sets of parameters considered above, the ratio of the shear to Doppler contributions is $\sim 6$. If instead we assume the same tilt for all species, as in the previous section, we should replace $\Omega_{\mathrm{b},0}$ by $\Omega_{\mathrm{M},0}$ in equation (67) and this ratio becomes $\sim 30$.

The effects of the improved treatment of tilt are thus twofold: (a) an increase in the relative level of the 'distorted dipole' to the 'distorted quadrupole' component in the temperature maps; and (b) a decrease in the overall level of polarization, given that the models are normalized to a fixed maximum $\Delta T/T$, and only the quadrupole at high redshift is responsible for producing polarization.

The revised temperature map and residual map for the $(x, \Omega_{\Lambda,0}, \Omega_{\mathrm{M},0}) = (0.62, 0, 0.5)$ model are shown in Fig. 5. The power spectra are plotted in Fig. 6. As expected, the polarization strength is somewhat lower after renormalization. The effects are in accordance with our expectations: the difference in the temperature maps amounts to a 15% effect, whilst the polarization level is reduced by approximately 10%.

It is clear that the details of how the tilt is treated will impact on a detailed statistical comparison of the models with the *WMAP* data, but a full study is beyond the scope of the present work. However these effects are not sufficiently large to make the Bianchi $B$-mode polarization unobservable at the three-year *WMAP* sensitivity (cf. Fig. 4), or change our overall conclusions.

## 6 CONCLUSIONS

We have derived the radiative-transfer equation for the CMB, including polarization, in all nearly-FRW Bianchi universes in the form of a hierarchy of multipole equations which can be easily integrated numerically. These can be coupled with the dynamical (i.e. Einstein) equations to compute maps of the CMB temperature anisotropies and polarization in any such model. $B$-mode polarization is generic, being produced in all Bianchi types except I. We applied these equations to the Bianchi VII$_h$ case, with parameters tuned to address the anomalous features observed in the CMB temperature on large scales (Jaffe et al. 2005, 2006). Our treatment includes a more physical treatment of the tilt velocity in CDM models with sub-dominant baryons. Whilst this does not make a qualitative difference to our results, more detailed statistical studies could well be affected by its $\sim 20\%$ corrections.

Our temperature maps are similar to those derived from earlier studies (Collins & Hawking 1973a; Barrow et al. 1985), although the amplitude is modified somewhat due to the better treatment of the ionization history. Polarization maps, with the generality presented here, do not appear to have been computed before. Note also that for these, a detailed treatment of recombination is required for accurate results. The power spectra of our type-VII$_h$ polarization maps apparently put these models in contradiction of the large-scale polarization results from *WMAP* (Page et al. 2007).

During the drafting of this paper, an analysis of universes equivalent to Bianchi I models, tuned to account for the low CMB quadrupole (Campanelli, Cea & Tedesco 2006), was shown to give a similar level of polarization to that computed here (Cea 2007). This is not surprising given that the anisotropies are tuned to address some of the same problems, and that the added complications induced by the VII$_h$ geometry do not substantially alter the amplitude of the effect (in the simplified dynamical model). In the type-I model, the temperature anisotropy and $E$-mode polarization are simply quadrupoles, and no $B$-modes are produced (see equation 52). Although the type-I model does not suffer the same observational constraints as type-VII$_h$ in polarization, the latter has the virtues in temperature of resolving essentially all of the large-angle anomalies.

Our cursory glance over the available data appears to rule out the VII$_h$ models employed in recent papers on the basis that they over-produce $B$-mode power. This is especially significant given that the results hold for all models on the Bianchi degeneracy line given in Jaffe et al. (2006). Our polarization results, combined with the failure of the Bianchi degeneracy region to include well-established values for the cosmological parameters, suggest that the simple VII$_h$ model, as it stands, is unsuitable to describe the available data. However, to reject completely the hypothesis that our universe contains anisotropic perturbations that are homogeneous under groups of motions with Bianchi type VII$_h$ requires a fuller treatment of the dynamics of the linearized model (Section 5.1). We intend to address this problem, and to search for statistical correlations between the morphology of the generalized model's polarization and the *WMAP* data, in future work.

## ACKNOWLEDGMENTS

AP is supported by a STFC (formerly PPARC) studentship and scholarship at St John's College, Cambridge. AC acknowledges a Royal Society University Research Fellowship. We thank Kendrick Smith, Antony Lewis and John Barrow for helpful discussions.

## REFERENCES

Barrow J. D., Juszkiewicz R., Sonoda D. H., 1985, MNRAS, 213, 917
Bianchi, I. 1897, Mem. Soc. Ital. Sci. Ser IIIa, 11, 267
Bridges M., McEwen J. D., Lasenby A. N., Hobson M. P., 2007, MNRAS, 377, 1473
Campanelli L., Cea P., Tedesco L., 2006, Phys. Rev. Lett., 97, 209903
Cea P., 2007, preprint (astro-ph/0702293)

Challinor A., 2000, Phys. Rev. D, 62, 043004
Collins C. B., Hawking S. W., 1973a, MNRAS, 162, 307
Collins C. B., Hawking S. W., 1973b, ApJ, 180, 317
Copi C. J., Huterer D., Schwarz D. J., Starkman G. D., 2007, Phys. Rev. D, 75, 023507
Dautcourt G., Rose K., 1978, Astronomische Nachrichten, 299, 13
Efstathiou G., Bond J. R., 1999, MNRAS, 304, 75
Ellis G., MacCallum M., 1969, Comm. Math. Phys., 12, 108
Ellis G., van Elst H., 1998, Arxiv preprint gr-qc/9812046
Estabrook F., Wahlquist H., Behr C., 1968, J. Math. Phys., 9, 497
Fabbri R., Tamburrano M., 1987, A&A, 179, 11
Fan X., Carilli C. L., Keating B., 2006, ARA&A, 44, 415
Goliath M., Ellis G. F. R., 1999, Phys. Rev. D, 60, 023502
Hawking S., 1969, MNRAS, 142, 129
Heckmann O., Schucking E., 1962, Gravitation: An Introduction to Current Research. Wiley New York, p. 438
Hu W., White M., 1997, Phys. Rev. D, 56, 596
Jaffe T. R., Banday A. J., Eriksen H. K., Górski K. M., Hansen F. K., 2005, ApJ, 629, L1
Jaffe T. R., Hervik S., Banday A. J., Górski K. M., 2006, ApJ, 644, 701
Lewis A., Challinor A., Lasenby A., 2000, ApJ, 538, 473
Lewis A., Challinor A., Turok N., 2002, Phys. Rev. D, 65, 023505
Loeb A., Zaldarriaga M., 2005, Phys. Rev. D, 71, 103520
MacCallum M. A. H., 1973, in Schatzman E., ed., Cargese Lectures in Physics, Vol. 6, p. 61
Matzner R. A., Tolman B. W., 1982, Phys. Rev. D, 26, 2951
Milaneschi E., Fabbri R., 1985, A&A, 151, 7
Misner C. W., 1968, ApJ, 151, 431
Page L. e. a., 2007, ApJS, 170, 335
Rees M. J., 1968, ApJ, 153, L1
Seager S., Sasselov D. D., Scott D., 1999, ApJ, 523, L1
Spergel D. N. e. a., 2007, ApJS, 170, 377
Taub A., 1951, The Annals of Mathematics, 53, 472
Varshalovich D. A., Moskalev A. N., Khersonskii V. K., 1998, Quantum theory of angular momentum. World Scientific: Singapore, 1988
Wainwright J., 1997, Dynamical Systems in Cosmology. Cambridge University Press
Wald R. M., 1983, Phys. Rev. D, 28, 2118